Electronic Supplementary Information

Reciprocal Redox Interactions of Lithium Cobalt Oxide Nanoparticles with Nicotinamide Adenine Dinucleotide (NADH) and Glutathione (GSH): Toward a Mechanistic Understanding of Nanoparticle-Biological Interactions

Austin H. Henke[†], Elizabeth D. Laudadio[†], Jenny K. Hedlund Orbeck[†], Ali Abbaspour-Tamijani[‡], Khoi Nguyen L. Hoang[§], Sara E. Mason[‡], Catherine J. Murphy[§], Z. Vivian Feng[£], Robert J. Hamers[†]*

[†]Department of Chemistry, University of Wisconsin, Madison, USA

[‡]Department of Chemistry University of Iowa, Iowa City, Iowa, USA

[§]Department of Chemistry, University of Illinois, Urbana-Champaign, USA

[£]Department of Chemistry, Augsburg University, Minneapolis, USA

*Corresponding Author, E-mail: rjhamers@wisc.edu

Contents:

Synthesis of $Co(OH)_2$ and $LiCoO_2$ nanosheets

We synthesized sheet-like nanoparticles of cobalt hydroxide, $Co(OH)_2$, and $LiCoO_2$ following procedures we described previously.[1, 2] $Co(OH)_2$ nanosheets were prepared via a precipitation method. First, 20 mL of 1 M $Co(NO_3)_2$ was added dropwise to a 0.1 M solution of LiOH and the precipitate was collected immediately after addition. The precipitate was isolated and washed by 3 repeated cycles of centrifugation for 5 min at 4696 × g (Thermo Scientific, Sorvall Legend X1) and resuspension in water. After washing, the supernatant was decanted, and the solid product was dried in a vacuum oven at 30 °C overnight. The $Co(OH)_2$ precursor was lithiated to form Li_xCoO_2 by to a molten salt flux of 6:4 molar ratio of $LiNO_3$:LiOH at 200 °C in a poly(tetrafluoroethylene) container with magnetic stirring in a silicone oil bath. After 30 min the reaction was quenched with water. The precipitate was isolated by decanting the supernatant, washed by 3 repeated cycles of centrifugation, and dried in a vacuum oven at 30 °C overnight.

Synthesis of $LiCoPO_4$ nanoparticles

As a control sample, we synthesized rod-like Cmcm $LiCoPO_4$ nanoparticles using a microwave-assisted solvothermal method adapted from a method published previously.[3] Successful synthesis of the Cmcm $LiCoPO_4$ polymorph is extremely sensitive to any contributions of moisture, and therefore all reagents were stored and handled in an argon-atmosphere glovebox. First, ~15 mL of tetraethylene glycol (TEG) was dried with anhydrous magnesium sulfate in an approximate 1:3 volume ratio. This solution was stirred for approximately 2.5 hr, allowed to settle overnight, and then decanted and centrifuged at 4696 × g for 10 min to fully separate out any remaining magnesium sulfate. Lithium hydroxide monohydrate, cobalt (II) acetate tetrahydrate, and anhydrous (solid) phosphoric acid were mixed in 1:1:1 stoichiometric ratio (2.38 mmol) in 12 mL of dried TEG in a 35 mL borosilicate microwave vessel and stirred overnight. Next, the mixture was removed from the glovebox and quickly loaded into a CEM Discover® SP microwave synthesizer equipped with Activent® capabilities to avoid over-pressurization. The microwave settings were set to 300 W, ~50 psi, and 260°C for 30 minutes with continuous high-speed stirring. The resulting pink/purple product was transferred from the microwave vessel to a 50 mL centrifuge tube and separated from the TEG solvent by centrifugation. After decanting, the product was washed in 3 cycles by suspending in ~20 mL acetone through mixing and ultra-sonication, and then centrifugation at 4696 × g for 10 min. Finally, the wash solution was decanted, and the particles dried in a vacuum oven at 30 °C overnight.

Chemical information and minimal medium with dextrose composition

Table S1. Reagent information.

Reagent	Supplier	Purity (%)
Magnesium chloride anhydrous	Alfa Aesar	99.0%
Dextrose (D-glucose)	Sigma Aldrich	99.5%
Indium foil	Sigma Aldrich	99.995%
Nitric acid	Sigma Aldrich	70.0%
Cobalt (II) choride hexahydrate	Sigma Aldrich	98.0%
Ammonium chloride	Sigma Aldrich	99.5%
NAD^+ free acid	Sigma Aldrich	99.9%
Ophthalmic acid	Sigma Aldrich	97.0%
L-Glutathione, reduced	Sigma Aldrich	98.0%
Tetraethylene glycol	Sigma Aldrich	99.0%
Magnesium sulfate	Sigma Aldrich	99.5%
Lithium hydroxide hydrate	Sigma Aldrich	98.0%
Cobalt (II) acetate tetrahydrate	Sigma Aldrich	98.0%
Anhydrous phosphoric acid	Sigma Aldrich	99.999%

Table S2. Composition of model bacterial growth medium “minimal medium” with dextrose used for nanoparticle dissolution experiments.

Component	Concentration (mM)
NaCl	11.6
HEPES	10.0
Dextrose (D-glucose)	10.0
KCl	4.0
Na_2SO_4	2.8
NH_4Cl	2.8
$MgCl_2$	1.4
Na_2HPO_4	0.088
$CaCl_2 \cdot H_2O$	0.051

Fluorescence and ICP-MS calibration

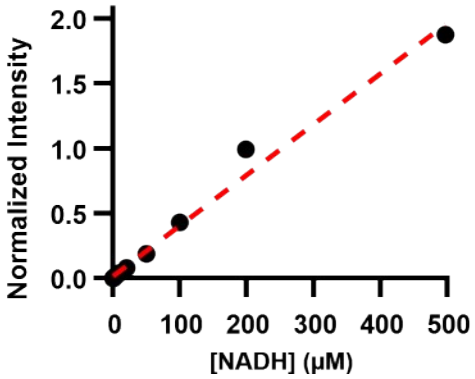

Figure S1. Fluorescence calibration curve of standard NADH solutions. Y = (0.00395 ± 0.00015)X, R^2 = 0.9850, n = 12.

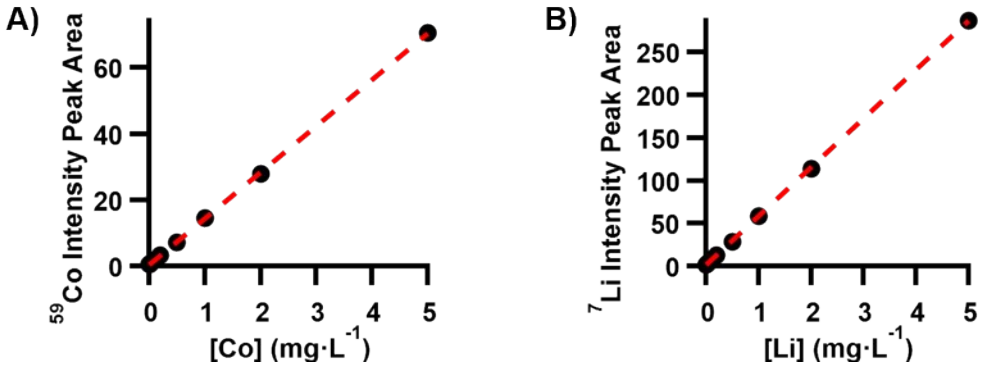

Figure S2. Representative ICP-MS standard calibration curves for quantifying A) Co, Y = (13.98 ± 0.04)X + (0.40 ± 0.08), R^2 = 0.99992, and B) Li, Y = (57.1 ± 0.2)X + (1.2 ± 0.3), R^2 = 0.99994. Standards were prepared by serial dilution from certified reference standards (1 g·L^{-1}, Sigma Aldrich).

TEM images of $LiCoO_2$ nanoparticles

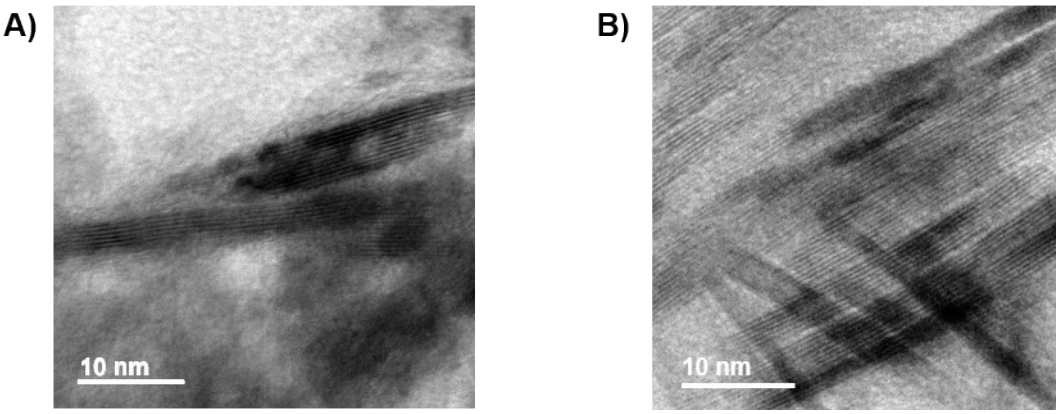

Figure S3. Transmission electron microscope (TEM) images of $LiCoO_2$ nanoparticles A) before and B) after exposure to minimal medium. Samples were washed twice for 20 min in nanopure water and drop-casted on a copper grid (Ted Pella, carbon type-B 300 mesh). Images taken on a JEO 2100 CRYO TEM with accelerating voltage at 200 kV and single-tilt holder.

Quantified [Li] release determined by ICP-MS

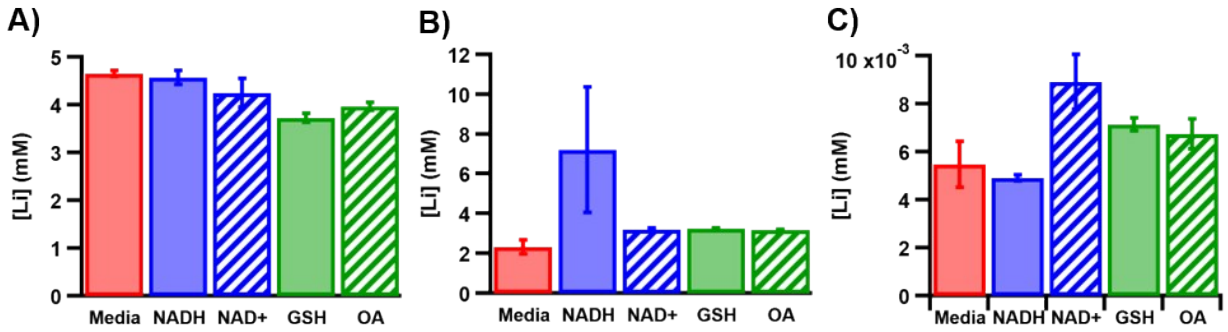

Figure S4. Dissolved Li concentrations in minimal medium solutions for A) $LiCoO_2$, B) $LiCoPO_4$, and C) $Co(OH)_2$ after 24-hr exposure to each molecule under study. A small amount of Li is present in $Co(OH)_2$ solutions as impurities within the synthesis (LiOH used to basify the solution) or within the commercial salts used to prepare minimal medium.

Changes in solution pH before/after nanoparticle exposure

Table S3. Measured pH of solutions containing the indicated molecule before and after 24 hr exposure to the indicated nanoparticles in minimal medium. Uncertainty for the pH probe used is estimated at pH ± 0.02.

Nanoparticle	Molecule	Initial pH	Final pH	ΔpH
$LiCoO_2$	None	5.33	7.15	1.82
$LiCoO_2$	NADH	5.18	7.32	2.14
$LiCoO_2$	NAD^+	4.61	7.16	2.55
$LiCoO_2$	GSH	4.52	7.16	2.64
$LiCoO_2$	OA	4.57	7.14	2.57
$Co(OH)_2$	None	5.33	7.50	2.17
$Co(OH)_2$	NADH	5.18	7.46	2.28
$Co(OH)_2$	NAD^+	4.61	7.44	2.83
$Co(OH)_2$	GSH	4.52	7.32	2.80
$Co(OH)_2$	OA	4.57	7.47	2.90
$LiCoPO_4$	None	5.80	6.85	1.05
$LiCoPO_4$	NADH	5.51	7.49	1.98
$LiCoPO_4$	NAD^+	4.63	6.74	2.11
$LiCoPO_4$	GSH	4.46	6.74	2.28
$LiCoPO_4$	OA	4.57	6.78	2.21

Additional control experiments regarding NADH fluorescence

First, we tested if dissolved Co^{2+} and Li^{+} ions alone (no particles) reproduced the decrease in [NADH] observed during $LiCoO_2$ dissolution, as this would suggest an aqueous phase reaction between the ions and NADH after nanoparticle dissolution. A 0.5 mM NADH solution was prepared with [Co] and [Li] typical after 24-h dissolution experiments (0.45 mM and 9.6 mM, respectively) from chloride salts. The fluorescence spectrum of this ion control solution after 24 h is nearly identical to that of the initial NADH solution (Figure S5A). Additionally, $Co(OH)_2$ releases similar amounts of Co to $LiCoO_2$ yet does not show the same dramatic decrease in [NADH] as with $LiCoO_2$. These data show that Li^{+} and Co^{2+} ions themselves have no effect on NADH concentration in our experiments.

Next, we were concerned that NADH might be lost during centrifugation steps or by molecules adsorbing onto the filter used during nanoparticle removal. To rule out this experimental error, a standard NADH solution (no particles) was treated in the same manner as unknown samples, including passing through the finely porous filter. The fluorescence spectra before/after passing through the filter are nearly identical (Figure S5B), showing that loss of NADH during the nanoparticle removal steps is minimal.

Removal of nanoparticles at the experiment stop time is necessary not only to halt dissolution, but also because nanoparticles would interfere with fluorescence analysis by absorbing and scattering light. To check that residual nanoparticles did not influence the experiment, nanoparticle dissolution samples without 0.5 mM NADH were analyzed by fluorescence. Samples without NADH yielded negligible fluorescence (Figure 4), as expected due to the lack of the fluorescent NADH. This eliminates the possibility of nanoparticles remaining in solution and interfering with NADH fluorescence spectra. NAD^{+} also contributes negligible fluorescence, as shown in Figure S7.

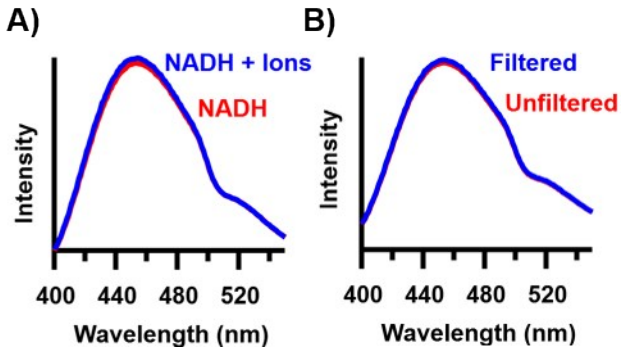

Figure S5. Fluorescence spectra of 0.5 mM NADH in minimal medium: A) after a 24-h period with (blue) and without (red) Co and Li ions, and B) before (red) and after (blue) filtration. There are no observed decreases in NADH fluorescence from filtration or exposure to Co^{2+} and Li^{+} ions.

Additional control experiments regarding NADH and NAD⁺ UV-visible absorbance

Standard solutions of NADH and NAD+ in minimal medium and pure water were analyzed by UV-visible spectroscopy. Using minimal medium vs. pure water as the solvent yields no difference in results if the same solvent is used as the blank. Serial dilutions were performed to prepare 9 samples ranging logarithmically in concentration from 1 – 500 µM (Figure S6A-B). Peaks are present at 203 nm, 259 nm, and 339 nm (NADH only). Absorbance values and linear least squares analysis were used to calculate molar absorptivities for both species at each wavelength (Table S4). Figure S7C illustrates each peak and compares absorbance for solutions of NADH and NAD⁺ at nominally the same concentrations. When the concentration of either species increases beyond ~200 µM, The 203 nm peak shifts to slightly higher wavelengths and the 259 nm peak splits in two (Figure S6D-E). In either concentration range, NADH and NAD⁺ both absorb similarly below 280 nm and NADH absorbs much more strongly above 300 nm.

Table S4. Molar absorptivities of NADH and NAD⁺ (1 – 100 µM) in pure water.

Species	$\varepsilon_{203\ nm}$ ($cm^{-1}\cdot M^{-1}$)	$\varepsilon_{259\ nm}$ ($cm^{-1}\cdot M^{-1}$)	$\varepsilon_{339\ nm}$ ($cm^{-1}\cdot M^{-1}$)
NADH	$(30.9 \pm 0.9)\times10^3$	$(13.1 \pm 0.1)\times10^3$	$(5.12 \pm 0.03)\times10^3$
NAD⁺	$(27.8 \pm 0.4)\times10^3$	$(15.3 \pm 0.3)\times10^3$	$(0.018 \pm 0.004)\times10^3$

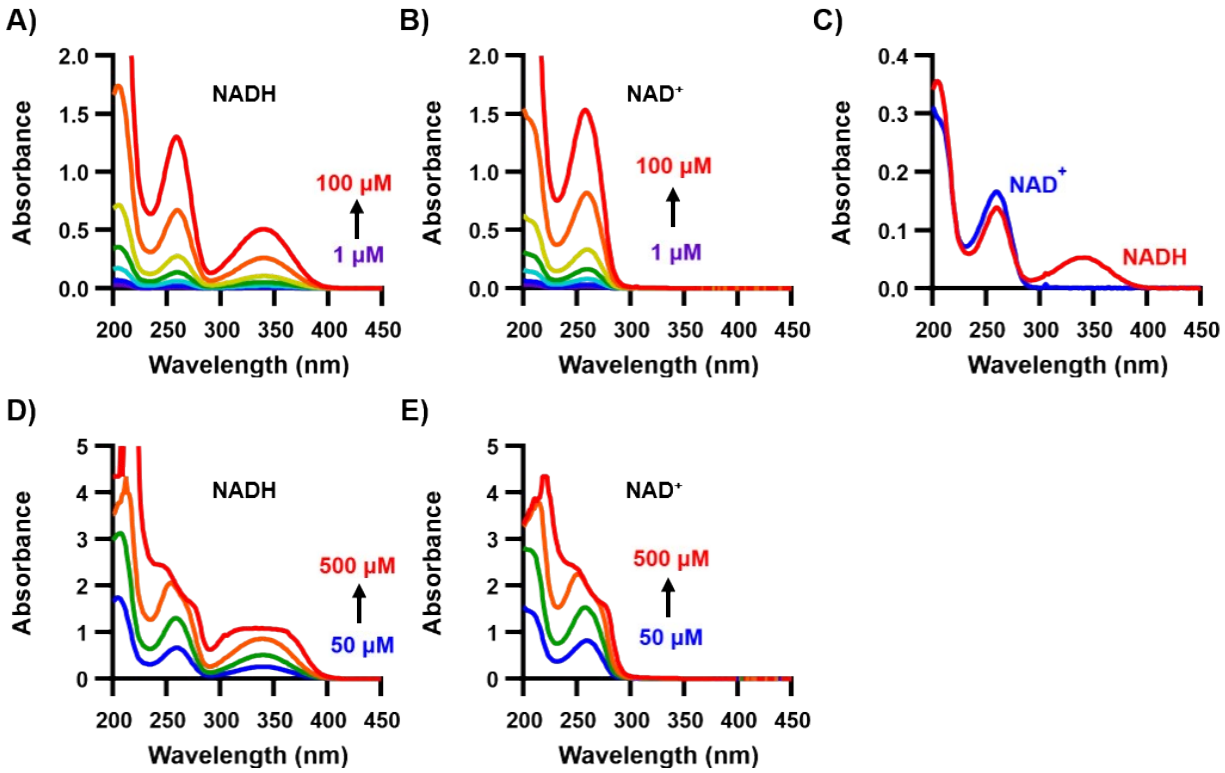

Figure S6. UV-visible absorbance spectra of standard solutions in nanopure water: A-B) NADH and NAD⁺ (respectively) in the linear range of 1 µM to 100 µM, C) 10 µM NADH and NAD⁺ spectra comparing absorbances at 259 nm and 339 nm, D-E) NADH and NAD⁺ (respectively) in a higher concentration range showing shifts in lower wavelength peaks.

Comparison of NADH and NAD^+ fluorescence spectra

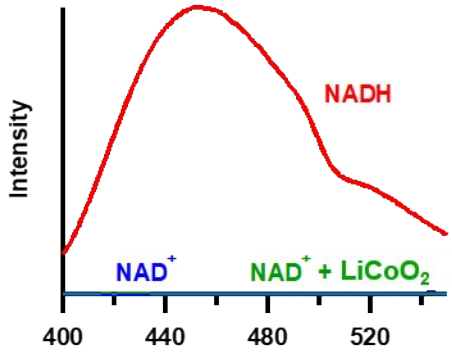

Figure S7. Fluorescence spectra of solutions containing NADH (red), NAD^+ (blue), and NAD^+ after 24-hr exposure to $LiCoO_2$ nanoparticles (green). Both NAD^+ solutions (blue and green) overlap near baseline, insignificant compared to NADH fluorescence.

Representative x-ray photoelectron spectra for NADH binding to nanoparticles

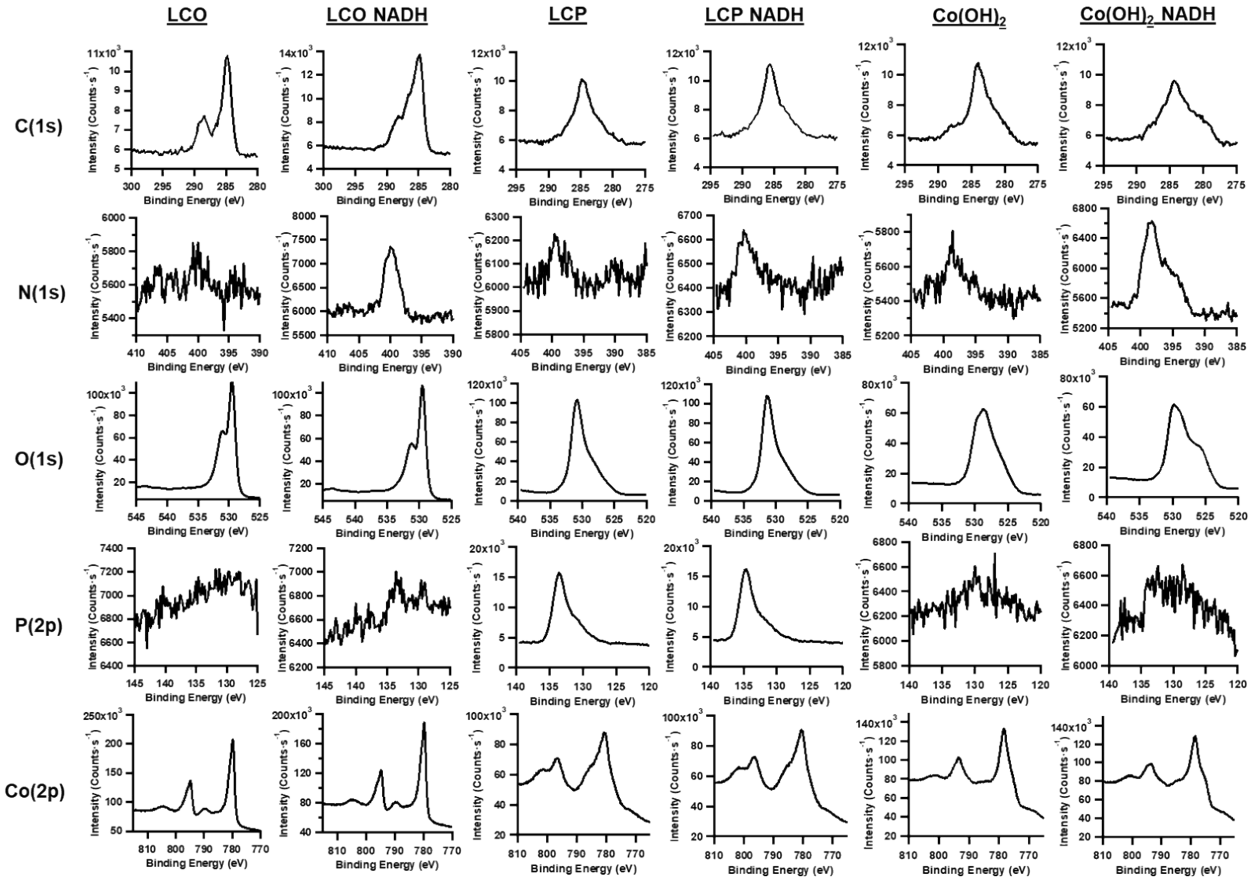

Figure S8. Representative XPS spectra for $LiCoO_2$ (LCO), $LiCoPO_4$ (LCP), and $Co(OH)_2$ nanoparticles pressed into indium foil after soaking for 24 hr in aqueous solutions with or without 0.5 mM NADH, arranged by the atomic transition measured. High-resolution spectra were obtained summing 10 (Co(2p)), 20 (O(1s) and C(1s)), or 50 (N(1s) and P(2p)) scans with step size of 0.2 eV and pass energy of 50 eV.

Description of XPS calculations

To quantify bound NADH on each type of nanoparticle, we first determine the N atom surface coverage using the following equation:

$$N\ coverage = \frac{A_{N(1s)}}{A_{Co(2p)}} \times \frac{SF_{Co(2p)}}{SF_{N(1s)}} \times \frac{scans_{Co(2p)}}{scans_{N(1s)}} \rho_{Co} \lambda_{Co(2p)} \cos\theta \qquad \text{Eq. S1}$$

Where $A_{N(1s)}$ and $A_{Co(2p)}$ are the areas for the respective peaks, $SF_{Co(2p)}$ and $SF_{N(1s)}$ are the sensitivity factors for the respective peaks ($SF_{Co(2p)}$ = 4.429 and $SF_{N(1s)}$ = 0.407), "scans" represents the number of scans summed for each peak, ρ_{Co} is the density of Co in the bulk, $\lambda_{Co(2p)}$ is the inelastic mean free path (IMFP) of Co(2p) electrons at the surface (estimated at 1.92 nm),[2] and θ is the angle of the analyzer relative to the surface normal (45°). This equation assumes the layer of NADH is thin relative to the electron IMFP and treats the bulk (Co) as an internal standard. The *molecular* coverage of NADH is obtained by subtracting the N coverage of samples not exposed to NADH and using the stoichiometry of 7:1, N atom to NADH molecule.

Determination of electrochemical potential for $LiCoO_2$ half reaction

The electrochemical potential for the reaction $LiCoO_2 + 4H^+ + e^- \rightarrow Li^+ + Co^{2+} + 2H_2O$ was determined using the free energy of formation of $LiCoO_2$, combined with known electrochemical reactions, as outlined below:[4]

$Li_{(s)} + Co_{(s)} + O_{2(g)} \rightarrow LiCoO_2$ $\Delta G^0 = -615\ kJ \cdot mol^{-1}$

$Co^{2+}_{(aq)} + 2e^- \rightarrow Co_{(s)}$ $E^0 = -0.28\ V$

$Li^+_{(aq)} + e^-_{(SHE)} \rightarrow Li_{(s)}$ $E^0 = -3.04\ V$

$O_{2(g)} + 4H^+_{(aq)} + 4e^- \rightarrow 2H_2O$ $E^0 = +1.229\ V$

Using $\Delta G = -nFE$, the electrochemical potentials are converted to free energies, with electrochemical potentials of electrons referenced to the standard hydrogen electrode, $\Delta G^0_{(SHE)}$

$Li_{(s)} + Co_{(s)} + O_{2(g)} \rightarrow LiCoO_2$ $\Delta G^0 = -615\ kJ \cdot mol^{-1} = -6.37\ eV$

$Co^{2+}_{(aq)} + 2e^- \rightarrow Co_{(s)}$ $\Delta G^0_{(SHE)} = +0.56\ eV$ as written

$Li^+_{(aq)} + e^- \rightarrow Li_{(s)}$ $\Delta G^0_{(SHE)} = +3.04\ eV$ as written

$O_{2(g)} + 4H^+_{(aq)} + 4e^- \rightarrow 2H_2O$ $\Delta G^0_{(SHE)} = -4.916\ eV$ as written

The overall reaction: $LiCoO_2 + 4H^+_{(aq)} + e^- \rightarrow Li^+_{(aq)} + Co^{2+}_{(aq)} + 2H_2O$ can then be written as

$LiCoO_2 \rightarrow Li_{(s)} + Co_{(s)} + O_{2(g)}$ $\Delta G^0 = +6.37\ eV$

$Co_{(s)} \rightarrow Co^{2+}_{(aq)} + 2e^-$ $\Delta G^0_{(SHE)} = -0.56\ eV$ as written

$Li_{(s)} \rightarrow Li^+_{(aq)} + e^-$ $\Delta G^0_{(SHE)} = -3.04\ eV$ as written

$O_{2(g)} + 4H^+_{(aq)} + 4e^- \rightarrow 2H_2O$ $\Delta G^0_{(SHE)} = -4.916\ eV$ as written

The sum of these reactions, and their corresponding energies, then leads to

$LiCoO_2 + 4H^+_{(aq)} + e^- \rightarrow Li^+_{(aq)} + Co^{2+}_{(aq)} + 2H_2O$

$\Delta G^0_{(SHE)} = +6.37 + (-0.56) + (-3.04) + (-4.916) = -2.14\ eV$

Finally, the standard electrochemical potential is determined as $E^0 = \Delta G^0_{(SHE)}/nF$ (here, n=1)

$LiCoO_2 + 4H^+_{(aq)} + e^- \rightarrow Li^+_{(aq)} + Co^{2+}_{(aq)} + 2H_2O$ $E^0_{(SHE)} = +2.14\ V$

Density functional theory (DFT) Computations

The free energy associated with the initial release of Co from $LiCoO_2$(001) surfaces was described previously.[5] Here we applied the identical methods and level of theory to determine the free energy associated with the initial release of Co from $LiCoPO_4$(010) surfaces. This approach couples first-principles calculations with thermodynamic experimental data. The overall dissolution process is following a two-step transformation. The starting surface is a $LiCoPO_4$(010) that has ½ monolayer of Li ions terminating the exposed surface. The half-monolayer Li termination corresponds to the surface that would be exposed by cleaving $LiCoPO_4$ along with (010) plane through a layer of Li atoms, with half the lithium atoms going to each of the two separating surfaces; this distribution of Li leads to free surfaces with zero net charge. In the first step, a Li/H ligand exchange occurs:

a. ½ Li-terminated $LiCoPO_4$ + 2H → ½ H-terminated $LiCoPO_4$ + 2Li Eq. S2

In the next step, a Co atom is removed from the ½ H-terminated surface, yielding a $LiCoPO_4$ with a surface Co vacancy, denoted as $LiCoPO_4$-vacancy:

b. ½ H-terminated $LiCoPO_4$ → ½ H-terminated $LiCoPO_4$-vacant + Co Eq. S3

This procedure does not remove a complete unit cell and therefore is distinct from the overall thermodynamic energy associated with complete dissolution of the material. We previously used similar methodology for $LiCoO_2$.[5] For $LiCoPO_4$ at pH = 7, our calculations yield ΔG for initial release of Co from the $LiCoO_2$(010) surface to be -0.87 eV. As a point of comparison, using the same methodology [5] for $LiCoO_2$ at the same pH and the removing the same fraction of Co atoms, the energy associated with initial release of a Co is +1.15 eV. This indicates that in pure water (i.e., in the absence of any reducing agents), the initial release of Co from the $LiCoO_2$(001) surface is much less favorable than release from the $LiCoPO_4$(010) surface.

Computational methodology:

Density functional theory (DFT) calculations were carried out using the Quantum Espresso open source suite.[6, 7] Exchange-correlation energies were approximated using GGA-PBE functional.[8] As pure DFT is known to over-delocalize the charge density, a remedial Hubbard *U* correction term of 5.00 eV magnitude was applied to Co^{2+} sites.[9-11] To describe atomic species GBRV ultra-soft pseudopotentials were employed.[12] In accordance with the criteria set for the pseudopotentials used, a plane-wave cutoff of 40 Ry for the wavefunction and 320 Ry for the charge density was selected for Kohn-Sham states. To account for the effect of unpaired electrons in Co(II), spin-polarization effects were included in the calculations. During the geometry optimization calculations, all the atoms in the structures were fully relaxed until the residual of forces was smaller than 5 meV·Å^{-2} per atom. For bulk calculations, the orthorhombic *Cmcm* phase of $LiCoPO_4$ was relaxed using a 6 × 4 × 6 grid of *k*-points and the obtained lattice constants were *a* = 5.54 Å (-2.21%), *b* = 8.29 Å (-1.59%), and *c* = 6.26 Å (-0.64%), in agreement with their experimental analogues of *a* = 5.42 Å, *b* = 8.16 Å and *c* = 6.22 Å.[13] The overprediction of the lattice constants by up to ~2% is attributable to the inherent shortcomings of the GGA-PBE exchange-correlation functionals. [14] The optimized bulk structure was cut along the (010) plane afterwards to create a P-1 slab possessing 3 Co layers. The resulting surface was expanded along the *y* axis to create a 1 × 2 supercell, providing four Co sites on each of its topmost layers (Figure S9). The generated slab has the dimensions of 6.26 × 11.07 × 12.57 Å^3. 25 Å of vacuum was inserted along the cleaved plane to evade undesirable interactions between periodic images

of surfaces exposed. A 4 × 4 × 1 and a 4 × 2 × 1 mesh was used to sample the reciprocal space for 1 × 1 and 1 × 2 slabs, respectively. All slab models have inversion symmetry and are optimized in accord with the best available practices for such calculations.[15, 16]

To quantify the energetics of dissolution, we turn our attention to ΔG of the cation release process. We use a combination of first-principles calculations and thermodynamics experimental data to obtain the cation release energetics. Our approach has, in the recent past, been successfully applied to several cases of release process in a wide variety of Li-ion rechargeable battery cathode materials, ranging from $LiCoO_2$ (LCO)[5] to $LiNi_{1/3}Mn_{1/3}Co_{1/3}O_2$ (NMC)[17] and its compositionally tuned variants.[18, 19] In this approach, we divide the overall ΔG into two sub-terms. $\Delta G1$ sub-term which accounts for the energy penalty to be paid to remove the transition metal from the lattice structure. This term is obtained by calculating the $\sum E_{products} - \sum E_{reactants}$ where DFT total energies are related to Gibbs free energies by accouting for zero-point energy and vibrational contributions, and all terms are purely DFT-calculable. As the (010) surface of $LiCoPO_4$ has an exposed layer of under-coordinated Co sites, the removal of this site dictates the magnitude of the $\Delta G1$**.** The thermodynamics pathway for this term starts with the surface terminated with a half-layer (50% occupancy) of Li atoms; this structure corresponds to the electrically charge-neutral surface that would be produced by cleavage through a layer of Li atoms, with half the Li atoms going to each opposing surface. In water, this surface undergoes a Li/H ligand exchange that leaves a ½ H-terminated surface, as shown in equation S2. In the next step, a cation is removed from the ½ H-terminated surface, yielding a $LiCoPO_4$ with a surface Co vacancy, denoted as $LiCoPO_4$-vacant, as shown in equation S3.

Since the created slab is a 1 × 2 supercell, it has 4 exposed penta-coordinated Co sites in its outermost layers (Figure S9). Therefore, the removal of one exposed Co from each side of the slab translates to a vacancy density of 25% per surface. Total ΔG_1 is the sum of the energetics of products minus those of reactants for the sum of steps a and b above, including the ZPE correction. The total energies of Li, Co, and H are computed based on their DFT atomic energetics predicted at their standard states, namely, $Li_{(s)}$, $Co_{(s)}$, and $H_{2(g)}$. The indirect outcome of this choice for the energetics of the elemental species, is that ΔG_1 is a measure of lattice stability upon the release of Co.

ΔG_2 which accounts for the energy given off upon the hydrolysis of released species is purely based on experimental data. This term is computed using the Nernst equation:

$$\Delta G_2 = \Delta G^0_{SHE} - n_e e U_{SHE} - 2.303 n_{H^+} k_B T pH + k_B T ln a^{z-}_{H_xAO_y} \qquad \text{Eq. S4}$$

In the above equation, ΔG°_{SHE} is the change in free energy of the aqueous species with respect to their standard states, referenced to the Standard Hydrogen Electrode (SHE). These values are tabulated in the literature.[20] We have also included them in Table S5. n_e is the number of electrons in the half-reactions for each species starting with their standard state, transforming to their oxidized forms under aqueous conditions. e is the charge of electron and U_{SHE} is the applied potential (set to zero here), n_{H+} is the number of protons associated with the oxidation chemical half-reactions considered for each species. $H_xAO_y^{z-}$ denotes the concentration of the constituent ions, assumed here to be 1×10^{-6} M, in line with the experimental data formerly reported for similar release experiments.[21]

In discussing the ΔG_2 terms, it is noteworthy that the values for Li^+ and Co^{2+} are the pH-independent while those of H and O, as H_2O, are pH-dependent. Table S5 contains the total

values of ΔG_2 various terms for the relevant species utilized in this work to predict the free energies of release from the $LiCoPO_4$ surface at neutral pH. Pourbaix diagrams show that $Li^+_{(aq)}$ and $Co^{2+}_{(aq)}$ are the dominant speciations for, respectively, Li and Co elements at up to neutral pH. The chemical reactions giving rise to ΔG^0_{SHE} for Li, H_2, Co, and O_2 are:

1. $Li_{(s)} \rightarrow Li^+_{(aq)} + e^-$

2. $½\ H_{2(g)} \rightarrow H^+_{(aq)} + e^-$

3. $Co_{(s)} \rightarrow Co^{2+}_{(aq)} + 2e^-$

4. $O_2 + 4H^+ + 4e^- \text{ --> } 2H_2O$

Table S5. Experimental[19] ΔG^0_{SHE} values of each aqueous species and their respective ΔG_2 at pH = 7.

Reactants	Product	ΔG^0_{SHE} (eV)	ΔG_2 (eV) at pH = 7
$Li_{(s)}$	Li^+	-3.039	-3.394
$H_{2(g)}$	H^+	0	-0.414
$Co_{(s)}$	Co^{2+}	-0.563	-0.918
½ O_2(g), $2H^+$	H_2O	-2.458	-1.632

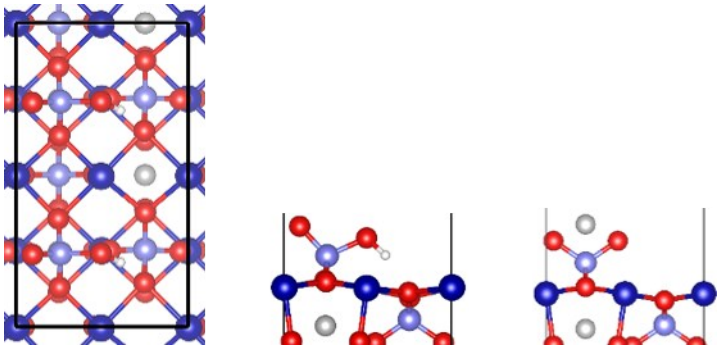

Figure S9. Top-view along *c* (left) and side-view along *b* (middle and right) of 1 × 2 supercells of ½ H-terminated (left and middle) and ½ Li-terminated (right) slabs used for surface calculations. Dark blue, light blue, grey, red and white spheres are Co, P, Li, O and H, respectively.

References

1. Laudadio, E. D.; Ilani-kashkouli, P.; Green, C. M.; Kabengi, N. J.; Hamers, R. J., Interaction of phosphate with lithium cobalt oxide nanoparticles: A combined spectroscopic and calorimetric study. *Langmuir* 2019, **35**, 16640-16649.
2. Laudadio, E. D.; Bennett, J. W.; Green, C. M.; Mason, S. E.; Hamers, R. J., Impact of phosphate adsorption on complex cobalt oxide nanoparticle dispersibility in aqueous media. *Environ. Sci. Technol.* 2018, **52**, 10186-10195.
3. Kreder III, K. J.; Assat, G.; Manthiram, A., Microwave-assisted solvothermal synthesis of three polymorphs of licopo4 and their electrochemical properties. *Chemistry of Materials* 2015, **27**, 5543-5549.
4. Wang, M.; Navrotsky, A., Enthalpy of formation of $LiNiO_2$, $LiCoO_2$ and their solid solution, $LiNi_{1-x}Co_xO_2$. *Solid State Ionics* 2004, **166**, 167-173.
5. Abbaspour-Tamijani, A.; Bennett, J. W.; Jones, D. T.; Cartagena-Gonzalez, N.; Jones, Z. R.; Laudadio, E. D.; Hamers, R. J.; Santana, J. A.; Mason, S. E., DFT and thermodynamics calculations of surface cation release in $LiCoO_2$. *Appl. Sur. Sci.* 2020, **515**, 145865.
6. Giannozzi, P.; Andreussi, O.; Brumme, T.; Bunau, O.; Nardelli, M. B.; Calandra, M.; Car, R.; Cavazzoni, C.; Ceresoli, D.; Cococcioni, M.; Colonna, N.; Carnimeo, I.; Dal Corso, A.; de Gironcoli, S.; Delugas, P.; DiStasio, R. A.; Ferretti, A.; Floris, A.; Fratesi, G.; Fugallo, G.; Gebauer, R.; Gerstmann, U.; Giustino, F.; Gorni, T.; Jia, J.; Kawamura, M.; Ko, H. Y.; Kokalj, A.; Kucukbenli, E.; Lazzeri, M.; Marsili, M.; Marzari, N.; Mauri, F.; Nguyen, N. L.; Nguyen, H. V.; Otero-de-la-Roza, A.; Paulatto, L.; Ponce, S.; Rocca, D.; Sabatini, R.; Santra, B.; Schlipf, M.; Seitsonen, A. P.; Smogunov, A.; Timrov, I.; Thonhauser, T.; Umari, P.; Vast, N.; Wu, X.; Baroni, S., Advanced capabilities for materials modelling with quantum espresso. *J. Phys.-Cond. Matter* 2017, **29**, 30.
7. Giannozzi, P.; Baroni, S.; Bonini, N.; Calandra, M.; Car, R.; Cavazzoni, C.; Ceresoli, D.; Chiarotti, G. L.; Cococcioni, M.; Dabo, I.; Dal Corso, A.; de Gironcoli, S.; Fabris, S.; Fratesi, G.; Gebauer, R.; Gerstmann, U.; Gougoussis, C.; Kokalj, A.; Lazzeri, M.; Martin-Samos, L.; Marzari, N.; Mauri, F.; Mazzarello, R.; Paolini, S.; Pasquarello, A.; Paulatto, L.; Sbraccia, C.; Scandolo, S.; Sclauzero, G.; Seitsonen, A. P.; Smogunov, A.; Umari, P.; Wentzcovitch, R. M., Quantum espresso: A modular and open-source software project for quantum simulations of materials. *J. Phys.-Cond. Matter* 2009, **21**, 19.
8. Perdew, J. P.; Burke, K.; Ernzerhof, M., Generalized gradient approximation made simple. *Phys. Rev. Lett.* 1996, **77**, 3865-3868.
9. Anisimov, V. I.; Solovyev, I. V.; Korotin, M. A.; Czyzyk, M. T.; Sawatzky, G. A., Density-functional theory and NiO photoemission spectra. *Phys. Rev. B* 1993, **48**, 16929-16934.
10. Anisimov, V. I.; Zaanen, J.; Andersen, O. K., Band theory and Mott insulators - Hubbard-U instead of Stoner-I. *Phys. Rev. B* 1991, **44**, 943-954.
11. Liechtenstein, A. I.; Anisimov, V. I.; Zaanen, J., Density-functional theory and strong-interactions - orbital ordering in Mott-Hubbard insulators. *Phys. Rev. B* 1995, **52**, R5467-R5470.
12. Garrity, K. F.; Bennett, J. W.; Rabe, K. M.; Vanderbilt, D., Pseudopotentials for high-throughput DFT calculations. *Comput. Mater. Sci.* 2014, **81**, 446-452.
13. Niggli, A., Die raumgruppe von Na_2CrO_4. *Acta Crystall.* 1954, **7**, 776-776.
14. Haas, P.; Tran, F.; Blaha, P.; Schwarz, K.; Laskowski, R., Insight into the performance of GGA functionals for solid-state calculations. *Phys. Rev. B* 2009, **80**, 13.
15. Corum, K. W.; Tamijani, A. A.; Mason, S. E., Density functional theory study of arsenate adsorption onto alumina surfaces. *Minerals* 2018, **8**, 18.
16. Tamijani, A. A.; Salam, A.; de Lara-Castells, M. P., Adsorption of noble-gas atoms on the TiO_2(110) surface: An ab initio-assisted study with van der Waals-corrected DFT. *J. Phys. Chem. C* 2016, **120**, 18126-18139.

17. Bennett, J. W.; Jones, D.; Huang, X.; Hamers, R. J.; Mason, S. E., Dissolution of complex metal oxides from first-principles and thermodynamics: Cation removal from the (001) surface of $Li(Ni_{1/3}Mn_{1/3}Co_{1/3})O_2$. *Environ. Sci. Technol.* 2018, **52**, 5792-5802.
18. Buchman, J. T.; Bennett, E. A.; Wang, C.; Tamijani, A.; Bennett, J. W.; Hudson, B. G.; Green, C. M.; Clement, P. L.; Zhi, B.; Henke, A. H.; Laudadio, E. D.; Mason, S. E.; Hamers, R. J.; Klaper, R. D.; Haynes, C. L., Nickel enrichment of next-generation nmc nanomaterials alters material stability, causing unexpected dissolution behavior and observed toxicity to *S. oneidensis* MR-1 and *D. magna*. *Environ. Sci. Nano* 2020, **7**, 571-587
19. Bennett, J. W.; Jones, D. T.; Hamers, R. J.; Mason, S. E., First-principles and thermodynamics study of compositionally tuned complex metal oxides: Cation release from the (001) surface of Mn-rich lithium nickel manganese cobalt oxide. *Inorg. Chem.* 2018, **57**, 13300-13311.
20. Wagman, D. D.; Evans, W. H.; Parker, V. B.; Schumm, R. H.; Halo, I.; Balley, S. M.; Churney, K. L.; Nuttal, R. L., NBS tables of chemical thermodynamic properties: Selected vaues for inorganic and C1 and C2 organic substances in SI units. *J. Phys. Chem. Ref. Data* 1982, **11**.
21. Huang, X.; Bennett, J. W.; Hang, M. N.; Laudadio, E. D.; Hamers, R. J.; Mason, S. E., Ab initio atomistic thermodynamics study of the (001) surface of $LiCoO_2$ in a water environment and implications for reactivity under ambient conditions. *J. Phys. Chem. C* 2017, **121**, 5069-5080.